International Journal of Thermal Sciences 208 (2025) 109489

Contents lists available at ScienceDirect

International Journal of Thermal Sciences

journal homepage: www.elsevier.com/locate/ijts

# Performance of photovoltaic panels with different inclinations under uniform thermal loading

Yu Wang [a,*], Chengming Xiao [a], Chiara Bedon [b]

[a] State Key Laboratory of Fire Science, University of Science and Technology of China, Hefei, 230026, PR China
[b] Department of Engineering and Architecture, University of Trieste, Trieste, Italy

ARTICLE INFO

*Keywords:*
PV panel fires
Different inclinations
Failure behavior
Uniform radiation
FEM model

ABSTRACT

Integrating photovoltaic (PV) panels with different tilt angles in building envelopes or roofs is widely employed for environmental sustainability. However, little is known about the influence of different tilt angles on the thermal failure of the photovoltaic façades or roofs in fire conditions. A total of 15 four-edge shielded PV panels ($300 \times 300 \times 4.7$ mm$^3$), with five different inclinations of 0°, 15°, 30°, 45° and 60°, were heated to fail using a uniform radiant panel. Measurements were taken to track glass thermal breakage, surface temperatures, incident heat flux and failure characteristics. The glass fracture and pyrolysis of the internal thermoplastic materials were observed under thermal radiation. The average breakage time of glass in PV panels showed an increasing trend with increasing inclination of the PV panels. Moreover, when the PV panels were tilted beyond 30°, the time to failure increased more significantly. The maximum temperature difference and heat flux that the PV panels can withstand were primarily measured within the range of 61–84 °C and 8–15 kW/m$^2$, respectively. Finally, the test results were simulated by a finite element method (FEM) model, calculating the heat transfer and thermal stress of PV panels: the average errors concerning temperature distributions and failure times were smaller than 15 % compared with the experimental results.

## 1. Introduction

Solar energy plays a significant role in the energy revolution due to its low cost and renewable energy potential. According to the International Energy Agency (IEA), at least 240 GW of photovoltaic (PV) systems were commissioned worldwide in 2022 [1], bringing the total number of photovoltaic installations to 1.2 TW. However, a land area equivalent to 0.3 % of the world is required if photovoltaic systems alone cover the global electricity demand [2]. Thus, the implementation of photovoltaic technology in buildings is an efficient way to transform passive areas into active parts with dual functionality. There are two primary forms of introducing a PV system into the built environment: building integrated PV (BIPV) systems and building applied PV (BAPV) systems. In BIPV systems, construction components can be replaced with PV modules with similar functions, while BAPV systems are not part of the construction but rather an "add-on" feature that can be removed without any significant consequences for the integrity of the host construction [3,4].

With the rapid increase in PV installations on buildings, there is a growing concern regarding potential risks associated with PV systems, particularly the risk of fire which escalates as the number of PV systems increases [5]. In August 2019, Walmart requested Tesla to eliminate PV panels from over 240 Walmart sites, and to pay damages resulting from the fires caused by the PV panels [6]. One of potential risks brought by this technology is the impact of PV panels and their mounting system on the combustibility of the roof and façade system since they alter the outside environment of the building. After analyzing over 50 PV fire events, the Building Research Establishment (BRE) revealed that these fires have caused damage to the PV installations themselves and to the buildings on which they are mounted [7]. Underwriters Laboratories (UL) conducted research tests [8,9] that validated this concern. They revealed that a PV panel could change the fire dynamics within a roof assembly, resulting in an escalated fire spread.

Regarding the fire safety of photovoltaic systems, there are two primary considerations: fires may be caused by the photovoltaic modules and modules themselves, called origin fire scenario; fires may be caused by external sources, known as victim fire scenario [10]. Ong et al. [11] used the fault tree analysis to investigate PV-related fire accidents in Australia, Germany, Italy, and the USA, and the qualitative results showed that electrical arcing is one of the main causes of fires. Lu et al.

* Corresponding author.
*E-mail address:* yuwang@ustc.edu.cn (Y. Wang).

https://doi.org/10.1016/j.ijthermalsci.2024.109489
Received 6 June 2024; Received in revised form 2 October 2024; Accepted 15 October 2024
Available online 24 October 2024

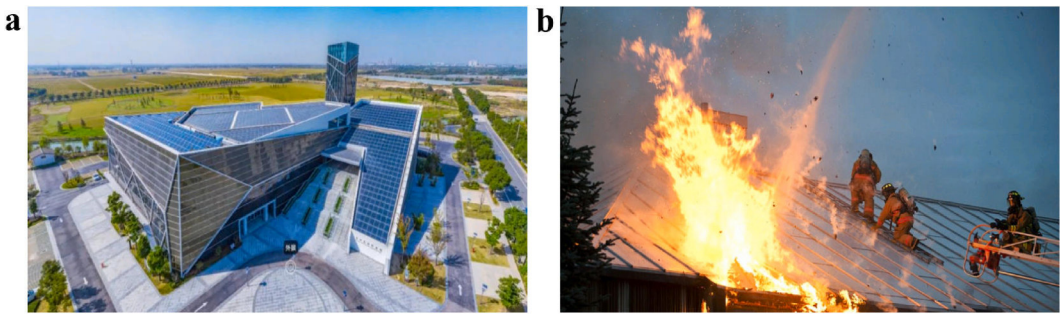

**Fig. 1.** (a) Photovoltaic curtain wall and roof in China [38]; (b) A photovoltaic fire at the inclined building roof [39].

[12] confirmed this reason, as they classified the types of arcing faults into series arcing, parallel arcing and grounding arcing, and found the high temperature generated by direct current voltage can easily cause PV fires. Another important reason for PV panel fires is related to the mechanism known as hotspots [13]. The hotspots on the PV module generate local heating on the back panel, which could not only enhance the energy loss but also ignite and cause fires [14]. The experiments conducted by Wang [15] showed that dust from the surroundings and some poor thermal objects attached to the PV cell surface could lead to the hot-spot phenomena. Furthermore, it is impossible to shut down the entire system to ensure that all components are powered off during a PV fire [16], and current continues to flow in the DC cable and the PV system continues to work during the burning, thus increasing severe electrical hazards for firefighters.

Another possible fire scenario, known as the victim fire scenario, also brings great risks. PV modules are made of some combustible materials, such as ethylene vinyl acetate (EVA) and Tedlar–Polyester–Tedlar (TPT), which may be ignited during fires. Relevant research has been conducted on the pyrolysis and combustion characteristics of these two materials. Hull et al. [17] investigated the combustion toxicity of EVA through a purser furnace under different fire conditions. Nair et al. [18] proposed an approach to assess the fire performance of different types of PV panel backsheets. Furthermore, when PV panels are installed on a building façade or roof, they add additional fuel load to the building, generating a large amount of heat and toxic gases under fire conditions [19,20] and hindering firefighting and rescue operations. In the past few years, fires in building photovoltaic systems around the world have been continually reported, causing severe personal injury and property damage; for example, PV-related fires were reported in the e-commerce company Amazon in 2018 [21], 2020 [22], and 2021 [23] (with the latter having an estimated cost of $500,000) and a PV system fire at an Apple Data Centre in 2015 [24]. In addition, PV modules also alter the existing structure, hence affecting fire dynamics when ignited. For example, the research conducted by Kristensen et al. [25–28] demonstrated that the bending flames beneath a PV panel from an incipient fire on a roof is a significant fire hazard in PV installations. Miao and Chow [29] built a combustion chamber connected to a vertical shaft to study the fire behavior of PV panels, which indicated that burning PV modules inside a cavity could exacerbate fire hazards.

However, the current status of establishing comprehensive protocols for fire tests on PV panels is still lacking [30]. Several standard tests have been established to evaluate the fire resistance of PV panels, such as the IEC 61730 Photovoltaic module safety qualification [3,31], the UL 1703 Flat-Plate Photovoltaic Modules and Panels [32] and the EN 50583 Photovoltaics in buildings [33]. IEC 61730 was issued by the International Electrotechnical Commission, while UL 1703, published by the Underwriter Laboratory, focused on fire security and reliability evaluations for PV systems. To simplify the rating process in IEC 61730, a method utilizing a propane torch as a fire source was proposed. These standards encompass a range of tests, including the temperature test (module safety test), hot-spot tolerance test, the ignitability test, bypass diode thermal test, and reverse current test [34].

Nevertheless, the performance of PV panels at different tilt angles has not been tested despite its widespread use and relevance. In practical engineering, PV panels are in fact mounted at different angles to optimize energy production and meet regulatory requirements, such as photovoltaic curtain walls, those inclinations generally between 0° and 15° are referred to as sloped glass curtain walls according to the technical specifications for glass curtain wall engineering (JGJ 102) [35]. Furthermore, roof-integrated PV panels are typically installed at yearly optimal inclinations to receive solar irradiance, with these angles rarely exceeding 60° according to practical building and prior research [36,37]. When a fire breaks out, due to the uncertainty of the roof slope, the PV panels will be heated at different inclinations, exacerbating the fire risk (see Fig. 1).

As revealed in previous studies, most conclusions tend to be focused on the quantitative correlation between the fire size [40] (such as the fire heat release rate) and the reradiation of flame under the PV panel. Little attention has been paid to the influence of the inclinations of PV panels on their behavior under fire conditions and fire hazard of building photovoltaic façades. The building façade would be an appealing surface after the installation of PV modules, which meanwhile may also pose fire risks. The serious accident at Grenfell Tower in London (UK) highlighted this risk, as the rapid propagation of flames through most sections of a building façade in a short time [41]. Bonner and Rein [42] observed an increasing trend in such fires, indicating growing complexity in design and technology for modern facades. The recent work by Stølen et al. [43] has confirmed the fire hazard, as they conducted a large-scale façade fire test (which was measured 4000 mm × 6000 mm and covered with PV panels) to investigate fire hazard of BIPV façade system, and found flame spread in the cavity and the integrity of the PV panel was compromised.

PV modules are composed of glass, which is widely used in modern architecture, despite its optical properties, it is a type of fragile material that may break or fall out quickly when subjected to fire [44–48]. As a consequence of glass cracks, the combustible materials of PV panels would directly receive fire radiation and access oxygen, facilitating the failure of PV systems. What is more, once the glass in the photovoltaic module breaks and falls out, the exposed component of the photovoltaic façade may transform into a large combustible surface, similar to the façade fires with thermal insulation materials, significantly exacerbating the fire risk of high-rise buildings. However, limited work has been performed to study the glass breakage under radiant heating [49,50], and even less for glass within PV modules in fire, although it plays an important role in the fire performance of PV panel and it façades.

In the current work, a total of 15 bench-scale experiments, including five different inclinations, were investigated to explore the thermal failure of PV panels. The PV panel frame and radiant panel were carefully designed to satisfy the experimental requirements, and the experiment primarily simulated the impact of an exterior fire on the front side (with glass), so the radiation source was normally located in front of the sample despite its inclination changed. Several critical parameters were

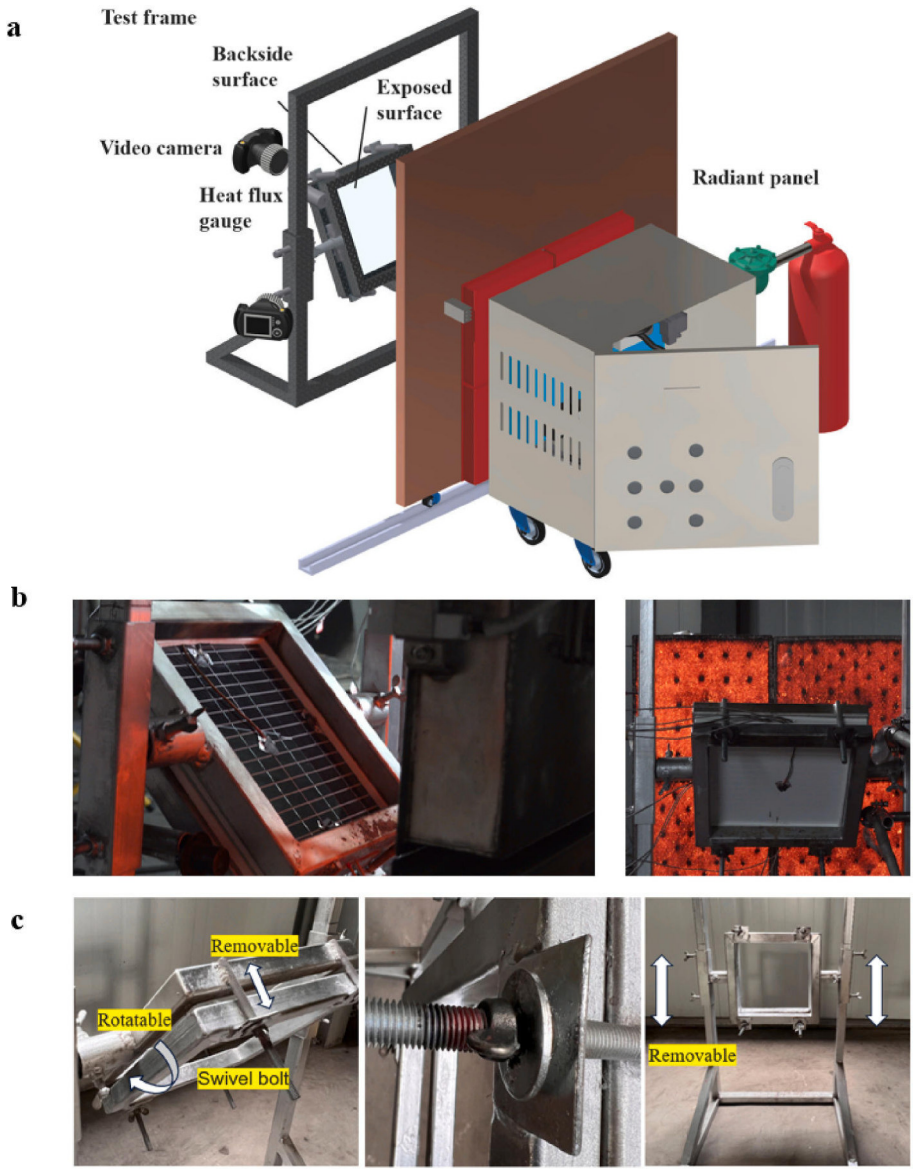


**Fig. 2.** (a) The experimental system; (b) Side and back photographs of the experimental setup; (c) The PV support frame.

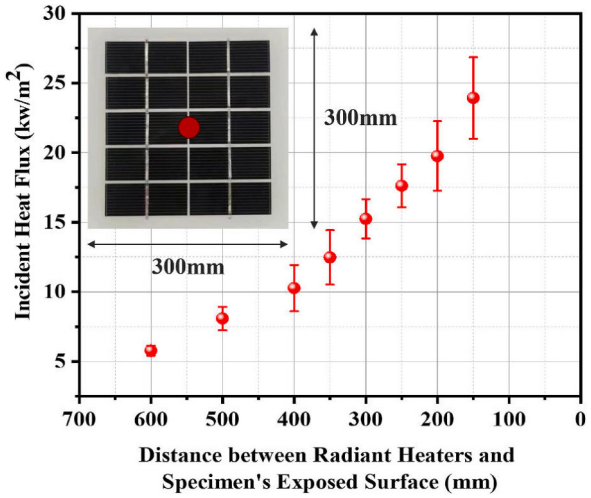


**Fig. 3.** The incident radiant heat flux calibration curve.

recorded, including crack initiation time, incident heat flux (HF) and surface temperatures. Moreover, based on the measured thermal loading, a finite element method model was used to predict the temperature distribution, stress distribution and breakage time. The experimental and numerical results are discussed in the following sections.

## 2. Methodology

### 2.1. Experimental system

As seen in Fig. 2(a) and (b), the experimental system comprised a uniform radiant panel and a test frame where the PV panels and the measuring setup were installed. The radiant array burns a compound of propane gas and air at a porous surface with 600 × 600 $mm^2$ dimensions. A Schmidt–Boelter heat flux gauge and two digital cameras were used in the test setup. The test frame can be adjusted vertically to align the PV panel center with the center of the radiant panel. In the experiments, a well-designed test frame made of galvanized steel square tubes, which could endure a temperature of 1200 °C, was used to install the PV panel. As depicted in Fig. 2(c), the frame was connected to the

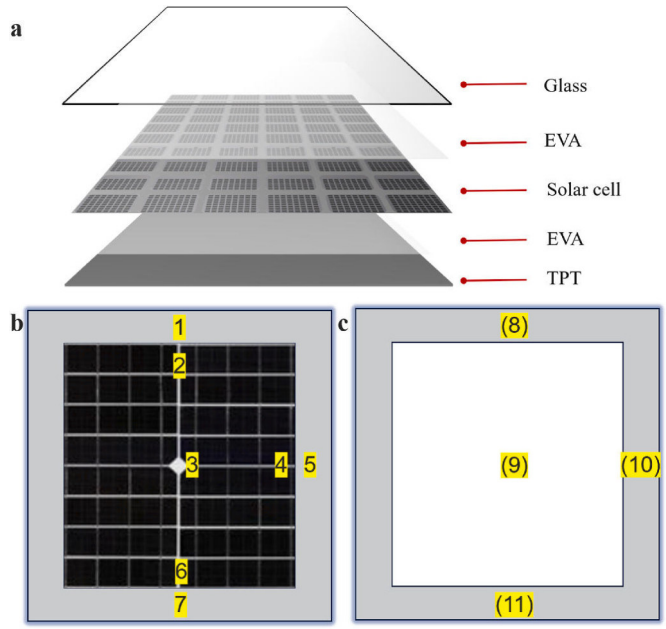


**Fig. 4.** (a) Structure of the photovoltaic panel; (b) and (c) Layout of thermocouples at fire exposed and ambient sides.

steel tube through internally welded bearings, allowing for adjusting the installation inclinations from horizontal to vertical (0–90° the tilt angle). In the thickness direction, each PV panel was clamped by the frame, and the clamping pressure was adjusted by rotating these screws, ensuring that the panel was rigidly constrained in the $x$, $y$ and $z$ directions. It is worth noting that the constraints in each experiment were ensured to be identical by marking the fixing position on the screw. The frame covered the outer 25 mm edge of the PV panel, creating a central heated area of 250 × 250 $mm^2$, while it did not restrict expansion in the plane due to the presence of a gap between the PV panel and the frame. 8-millimeter-thick ceramic fiber papers were covered with the edges of the PV panel and secured into the test frame. The ceramic fiber paper insulated the edge of the PV panel from the test frame and may as well prevented localized stresses of uneven pressure from the frame. Simultaneously, the height of the experimental frame can be vertically adjusted to ensure that the sample was heated from the center of the radiation panel.

The radiant panel comprised four high-performance methane gas-fired radiant heaters (300 × 300 $mm^2$ each), forming a 600 mm × 600 $mm^2$ radiant heat source. During preliminary tests, a water-cooled heat flux gauge was employed to measure the incident radiant heat flux of the exposed surface of the specimen. The calibration graph in Fig. 3 illustrates the incident radiant heat flux between radiant panel and specimen's exposed surface. The error bars indicate the deviation of heat flux from 3 repeated calibration tests. The PV panel was positioned in parallel with the radiative panel with a distance of 25 cm, which was demonstrated to be suitable for inducing cracking through pre-testing.

In this study, sheet thermocouples (TCs) were attached to both the PV panel front and back surfaces at different positions, to measure the temperature through high heat-conducting sheets, which were composed of a highly conductive aluminum alloy [51]. With dimensions of 20 × 10 $mm^2$, the thermocouples increased contact areas between the temperature-sensing elements and the detected objects. The measurement of thermocouples ranges from 0 to 800 °C, which is adequate for conducting these tests. Thermocouples were set at the three edges of the PV panel, the three-sided shielding area and the geometric center, as shown in Fig. 4. For the purpose of analysis, unbracketed numbers represent the thermocouples attached to the sides exposed to fire, whereas bracketed numbers indicate the thermocouples situated on the ambient sides. As discussed, a heat flux gauge was positioned towards the radiant panel and adjacent to the top of the PV panel. As the inclination of the PV panel changed with the test frame, the position of the heat flux gauge also changed and remained flush to the surface of the PV panel accordingly.

### 2.2. Test procedure

To ensure a consistent level of emitted radiation from the radiant panel, the central heat flux of the radiation panel was measured using a

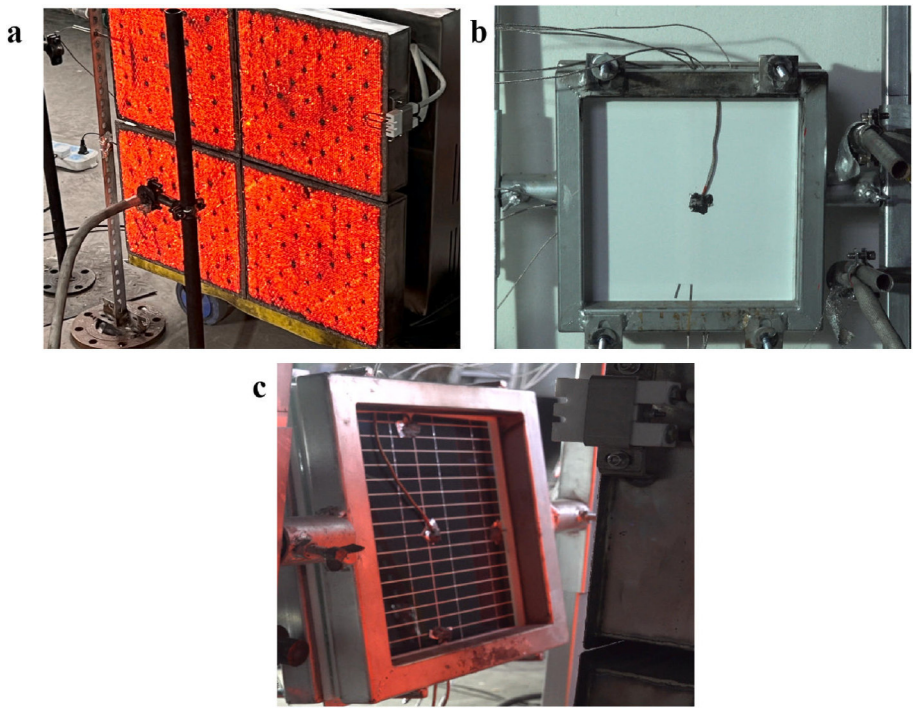


**Fig. 5.** Experimental steps: (a) Measurements without the PV panel in position; (b) Warm-up of the radiant array (back view); (c) Side view of the PV panel exposure.

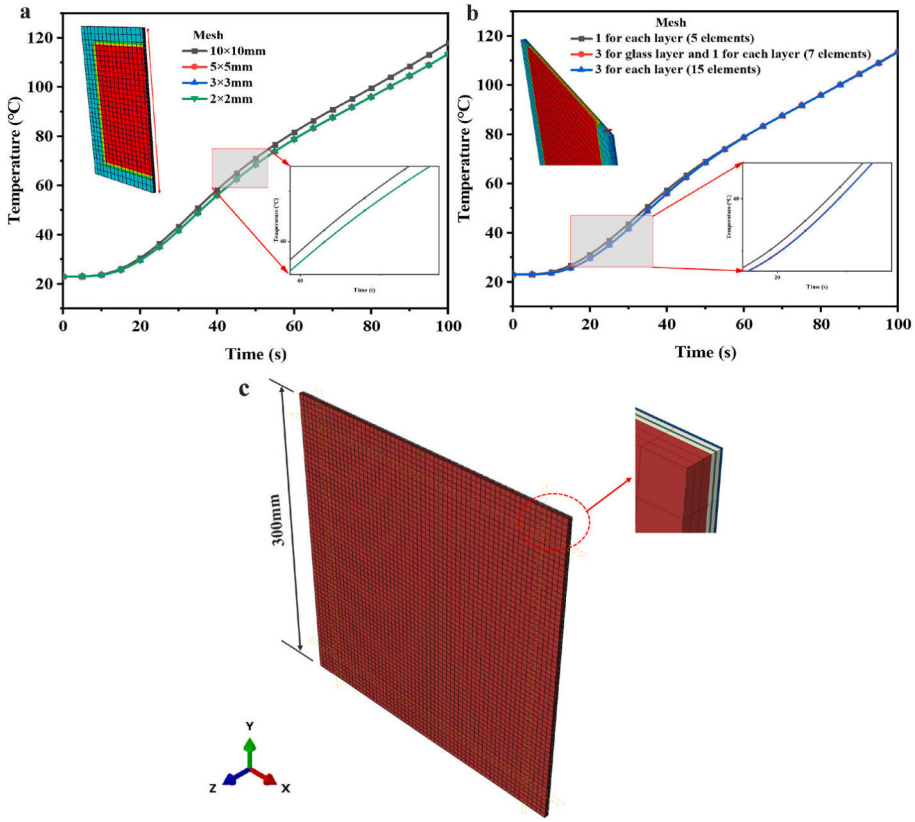


**Fig. 6.** (a) Temperature curves with different meshes on the planar direction; (b) Temperature curves with different meshes along the thickness direction; (c) The numerical model.

heat flux gauge before each test (see Fig. 5(a)). As illustrated in Fig. 5(b), before the test, an insulating board was positioned in front of the PV panel to prevent it from being heated when the radiation panel was warming up. Once reaching the targeted incident heat flux, the insulating board was taken away to allow the PV panel to be directly exposed to the radiation source, as seen in Fig. 5(c). Two video cameras, one on the side of the sample and the other on the back were used to record the experiments at a rate of 25 frame/s, and the timings of events such as PV glass breakage and melting of the backplate could be measured accurately from the video footage. In each test, high-resolution photographs (3840 × 2160 pixels) were captured to document the radiation-exposed and ambient sides of the PV panel.

The common forms of combining PV modules into buildings include PV curtain walls, roofs, and sunshades. Based on the Chinese industry standard for glass for solar cell modules, glass for PV panels can be divided into tempered glass and non-tempered glass. In this study, a typical monocrystalline silicon PV panel (300mm × 300 mm), which has five layers from face to rear, including, 3.2 mm thick annealed (non-tempered) glass layer, EVA layer, monocrystalline solar cell layer, EVA layer and TPT dorsal membrane, was selected; five different inclinations of 0°, 15°, 30°, 45° and 60° were set respectively according to real situations. Since it is typical for tiny flaws to exist in glazing for PV panels, the occurrence of glass pane cracking when exposed to fire is random [46,52,53], thus three replicate experiments were performed for each group. All 15 tests were controlled under identical thermal conditions.

**Table 1**
Physical properties of each layer in the PV panel [57–60].

| Properties | Value |
|---|---|
| Glass | |
| Density (kg/m$^3$) | 2600 |
| Thermal expansion coefficient (1/K) | $8.46 \times 10^{-6}$ |
| Modulus of elasticity (Pa) | $6.7 \times 10^{10}$ |
| Poisson's ratio | 0.22 |
| Specific heat capacity (J/(kg·K)) | 835 |
| Thermal conductivity (W/(m·K)) | 0.95 |
| EVA | |
| Density (kg/m$^3$) | 980 |
| Specific heat capacity (J/(kg·K)) | 2300 |
| Poisson's ratio | 0.3 |
| Modulus of elasticity (Pa) | $10^7$ |
| Thermal conductivity (W/(m·K)) | 0.2 |
| ELE | |
| Density (kg/m$^3$) | 2400 |
| Specific heat capacity (J/(kg·K)) | 2030 |
| Poisson's ratio | 0.22 |
| Modulus of elasticity (Pa) | $1.3 \times 10^9$ |
| Thermal conductivity (W/(m·K)) | 100 |
| TPT | |
| Density (kg/m$^3$) | 1780 |
| Specific heat capacity (J/(kg·K)) | 1210 |
| Poisson's ratio | 0.35 |
| Modulus of elasticity (Pa) | $2.2 \times 10^8$ |
| Thermal conductivity (W/(m·K)) | 0.13 |

### 2.3. Finite element method

A FEM model was developed in ABAQUS [54] to calculate the temperature distribution and the first failure time of the exposed PV panel. The numerical model was the same as the experiments, which measured 0.3 × 0.3 m$^2$ with a thickness of 4.7 mm. Since the temperature difference between the exposed and unexposed areas had a significant impact on panel failure, the simulation model primarily focused on thermo-mechanical processes. In preliminary calculations of the model, the number of mesh sizes was considered. To analyze the temperature gradient in the planar direction, four different element sizes were chosen: 10, 5, 3, and 2 mm. It can be seen from Fig. 6(a) that the planar

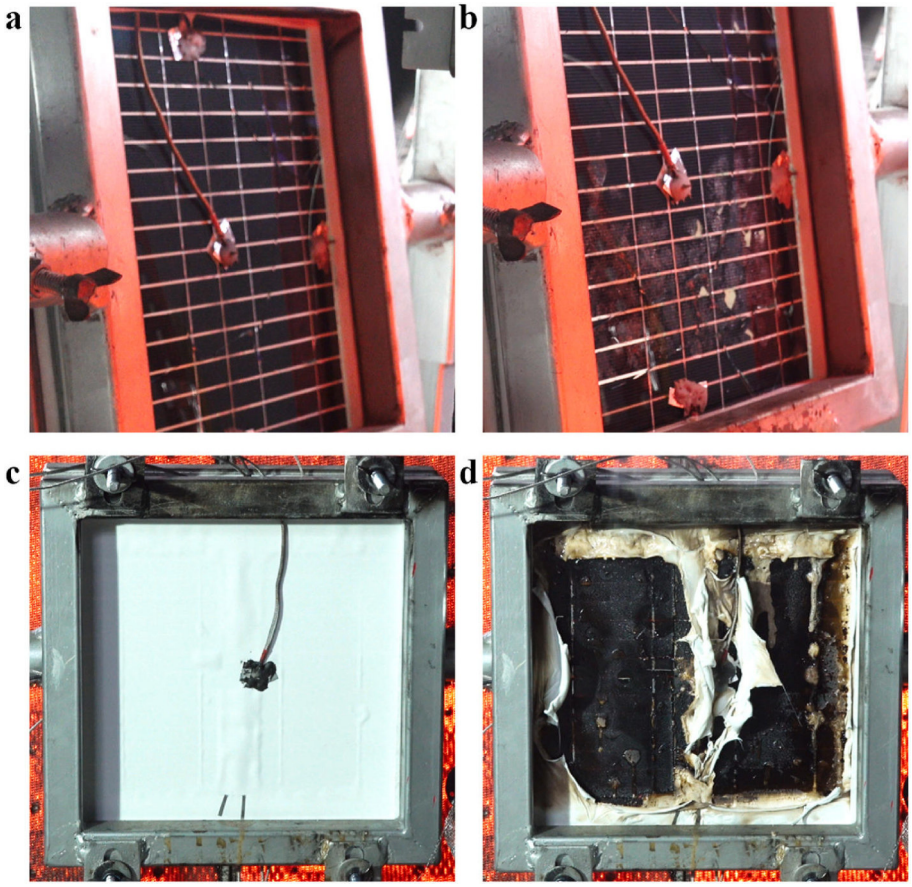


**Fig. 7.** (a) Glass breakage in the PV panel; (b) and (c) Gas bubble initiated between the solar cell layer and the float glass, and between the TPT and the solar cell layer; (d) Discolouration and charring of the TPT.

temperature curve changes by less than 3.3 % when the element size decreased to 5 mm, whereas a further reduction to 2 or 3 mm did not bring in significant improvements (differences in temperature distribution less than 0.01 %) with a significant increase of computational time. Therefore, an element size of 5 mm along the length and width was sufficient for the PV panels heat transfer model. In the thickness direction, the glass layer was usually divided into three elements [55], and the temperature profiles at the center of the back sheet were similar when the elements changed from five elements to fifteen elements, as demonstrated in Fig. 6(b). Consequently, with seven elements along the z-axis (three for the glass layer and one each for the EVA, ELE and TPT layers), the total number of elements was 25,200, as illustrated in Fig. 6 (c).

A heat transfer model based on eight-node solid elements (DC3D8) was developed. The material properties of float glass, EVA, solar cell and TPT are listed in Table 1, which are utilized in both heat transfer and structural models. Note that the variation of material properties with temperature was disregarded. Also, the heat exchange between the PV panels and the surrounding environment was assumed to solely occur on the back sheet through convection and radiation during the fire. The values assigned for the convection coefficient and effective emissivity factor were 10 W/(m2·K) and 0.89, respectively [56]. The thermal boundary conditions were taken as the average temperature in the covered area (T1, T5 and T7) and the exposed area (T2, T3, T4 and T6). The thermal stresses were worked out via the sequentially-coupled thermo-mechanical analyses, which were in accordance with the same element size of the heat transfer model. In the extended finite element method (XFEM) enriched region, the first failure time of glass in PV panels was predicted using the maximum principal stress (Maxps) damage initiation principle.

**Table 2**
First failure time and standard deviation of the tested photovoltaic panels.

| Experimental Conditions | First failure time (s) | | | | |
|---|---|---|---|---|---|
| | Test 1 | Test 2 | Test 3 | Average | Standard deviation |
| Case 1 (0°) | 38 | 32 | 37 | 36 | 3.2 |
| Case 2 (15°) | 34 | 29 | 36 | 33 | 3.6 |
| Case 3 (30°) | 38 | 46 | 36 | 40 | 5.3 |
| Case 4 (45°) | 72 | 60 | 54 | 62 | 9.2 |
| Case 5 (60°) | 77 | 68 | 67 | 71 | 5.5 |

## 3. Results and discussion

### 3.1. Experimental results

#### 3.1.1. Thermal behavior and failure time

For photovoltaic panels exposed to constant heat flux, the experimental phenomena were consistent across different experimental conditions. In all experiments, it was observed that the glass first fractured (Fig. 7(a)). Subsequently, a chemical reaction occurred within the EVA interlayer, and gas bubbles were formed (Fig. 7(b)). These gas bubbles were generally found between the glass layer and the solar cell layer, as well as between the backplate and the solar cell layer. As the test continued and the reaction proceeded, the gas bubbles gradually became larger and more widespread. These bubbles contained combustible pyrolyzed gases, which were observed releasing from cracks when the bubble was broken. Furthermore, on the rear of the PV panel, the thermal expansion of the TPT dorsal membrane was initially

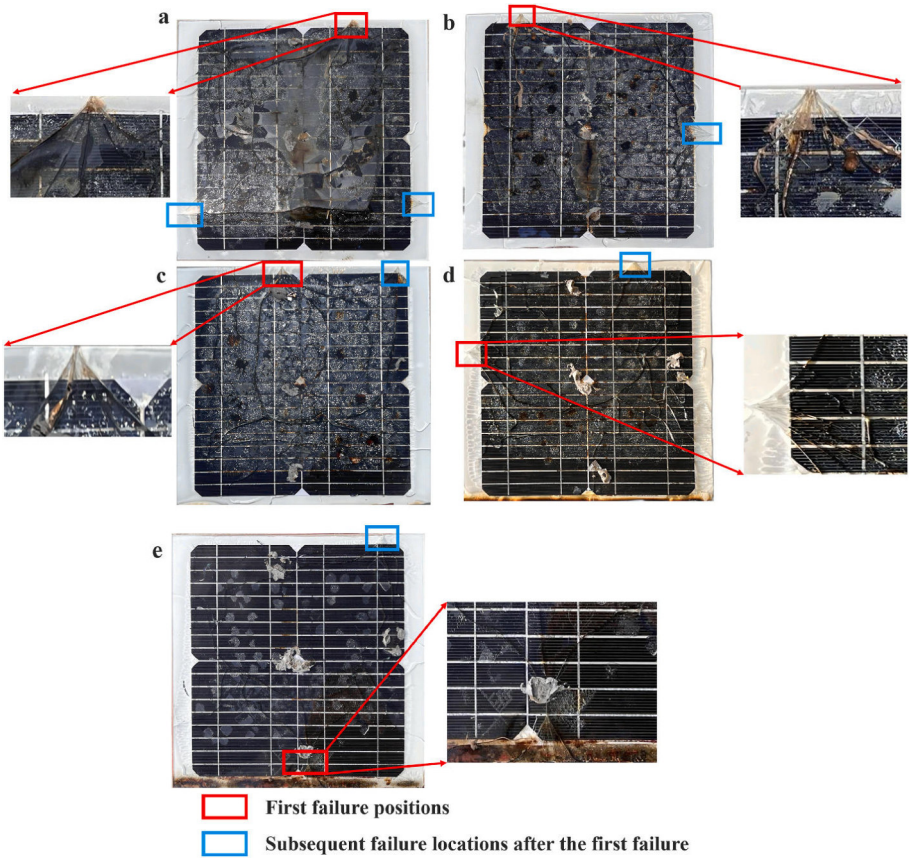


**Fig. 8.** Failure positions of the PV panels. (a) Test 2 (Case 1, 0°); (b) Test 3 (Case 2, 15°); (c) Test 2 (Case 3, 30°); (d) Test 1 (Case 4, 45°); (e) Cracks at the intersection of the shaded and exposed areas in Test 3 of Case 5 (60°).

observed, generating small bubbles (Fig. 7(c)), which correlated with the pyrolysis of EVA or TPT. Next, the TPT decomposed, resulting in the emission of a substantial amount of combustible gas, which could be ignited if a sparker was put there (confirmed in a pre-test). In the later period, as illustrated in Fig. 7(d), the TPT melted and dripped continuously, while the dorsal membrane was carbonized and discolored, as shown in the attached video.

In this experiment, 0° was defined as vertical and the time of the first glass crack occurrence was defined as the failure of the PV panel, which indicated the structural failure of the PV panel, resulting in the combustible materials directly radiated by the fire and access to the oxygen for ignition and burning. All 15 PV panels shattered during the fire, and the first failure times and standard deviation are summarized in Table 2. The average time for photovoltaic panels first failure generally showed an increasing trend when the panel inclined from 0° to 60°. When the inclinations were 0° and 15°, the difference in the first failure time was not significant due to the relatively small variation in inclinations. After the crack originated at the side of the photovoltaic panel, a larger area of island cracks was formed, followed by rapid vertical development at the side of the glass and at the bottom of the island cracks along the left and right edges. However, when the PV panel was further tilted beyond 30°, the overall radiative heat on the PV panel surface decreased, with the average total heat flux decreased from 11.3 to 9.9 kW/m$^2$ from 30° to 45°; meanwhile the time to failure increased 55 % due to the increased inclination reduction of the view factor and decreased imposed heat flux. Therefore, 30° can be taken as a critical point for the failure time of the PV panel.

Once tensile stress surpasses glass strength, cracks may be initiated. Regarding the initial point of failure for PV panels, which can be seen in Fig. 8(a)-(d), the preponderance of experimental failure positions were mostly located at the upper edge and the left and right edges due to the rising effect of hot air. However, it is noteworthy that in Test 3 of Case 5 (Fig. 8(d)), the first crack was initiated at the intersection of the shaded and exposed areas rather than panel edges; similar crack initiation locations were also found in Test 2 and 3 of Case 4 (not first crack), which suggests that as the inclinations increased, the distance between the lower part of the PV panel and the radiation panel decreased, then the radiator may heat the aluminum solder ribbons directly. These ribbons were soldered directly onto silicon crystals to interconnect solar cells in the PV panel, and converged at the intersection of the shaded and exposed areas, where the heat was accumulated, ultimately leading to the cracking of the PV panels. Owing to the inclined orientation of the PV panels, the thermal radiation effect was attenuated. Consequently, compared with those in the other cases, the number of glass cracks and the degree of back sheet failure in Cases 1, 2 and 3 were significantly greater.

### 3.1.2. *Temperature and heat flux distributions*

The temperature change of the PV panel surface under thermal loading is an important parameter for describing the breakage behavior of the panel. The temperatures of surface and backplate of PV panels in each case are shown in Fig. 9 (the thermocouple distribution available in Fig. 4), and the dotted lines represent the different failure times of the PV panels. The diagrams illustrate that temperatures in exposed areas are significantly higher than those in covered areas: TCs 2, 3, 4 and 6 were directly exposed to the radiant panel, resulting in a rapid temperature increase. Simultaneously, at the moment of initial failure of the PV panel, the temperature curve exhibited a sudden change, leading to a deceleration in the rate of temperature growth, which may be caused by the stronger thermal decomposition of EVA (an endothermic reaction [61], in which energy was absorbed when the bonds were broken). At the same time, there was an inflection point in the temperature curve,

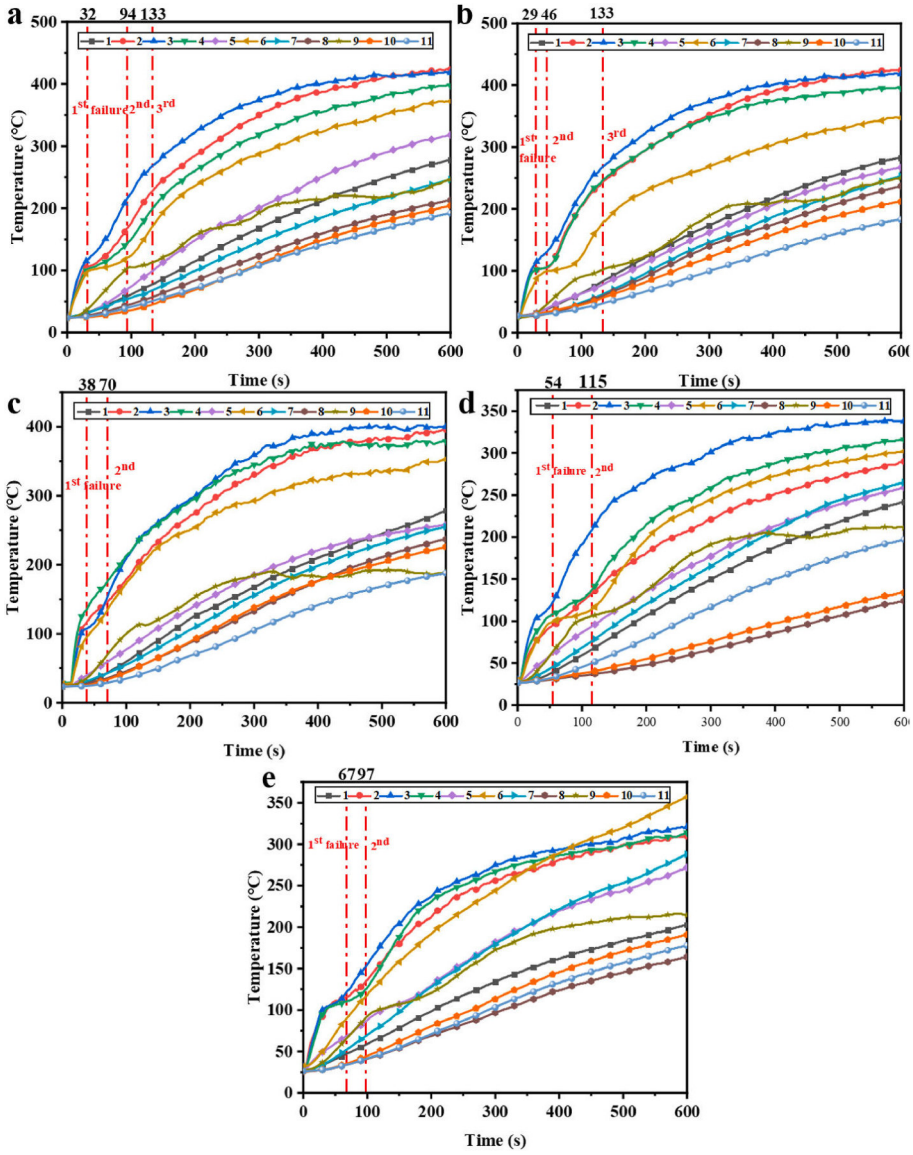


**Fig. 9.** Temperature of thermocouples at different positions. (a) Test 2 (Case 1); (b) Test 2 (Case 2); (c) Test 1 (Case 3); (d) Test 3 (Case 4); (e) Test 3 (Case 5).

and the rate of temperature increase slowed down at the moment of the first failure. Similarly, the temperatures measured by TCs 1, 3, 7 and 9, which were situated in sheltered regions, increased significantly more slowly compared with the exposed temperatures. While TCs 8, 10 and 11 were set on the backside surface, the measured temperatures were approximately linear with respect to time, as shown in Fig. 9, which indicates that the backside surface was mainly heated by heat conduction from the fire exposed surface and was not affected by the thermal radiation of the fire source. Furthermore, noting that the temperature measured by TC 9 after the expansion and pyrolysis of TPT is that of the gases rather than the back sheet. Throughout most of the heating period, the temperatures at the center in exposed areas were the highest of all measured positions, both on the fireside and backside surfaces. As the inclinations increased, the upper incident heat flux of the PV panel decreased, leading to a corresponding temperature decrease, and the temperature of TC 4, located to the right of the center, did not exceed that of TC 2 until the inclination reached 45°. When the inclination was 60°, the rate of temperature increase measured by the bottom TC 6 was notably higher than those in the exposed areas after the photovoltaic panel failed.

The local high stress caused by the temperature difference is the main cause of glass breakage within PV panels; therefore, under this heat condition, the temperature difference at the three shielded edges of the PV panel, the temperatures of the fireside and the backside and the maximum temperature difference in exposed areas are important parameters to characterize the development of PV panel fires. As shown in Table 3, most of the PV failure panel locations were located at the edge of the maximum temperature difference on the fireward surface (noted that some tests were at the left edge where temperatures were not measured in all tests), and the maximum temperature difference mainly occurs in the upper and middle part of the PV panel. This may be attributed to the fact that the air is heated by the heat source and the upper air temperature is relatively high, resulting in a large temperature difference between that point and the shelter. Although the failure times were very different under different conditions, the average temperature differences remained close, ranging from 62 to 84 °C.

Another significant factor for PV panel failure is the total heat flux. The water-cooled heat flux gauge was located near the PV panel but flush to the upper part of the panel surface. Fig. 10 illustrates the variability of the incident heat flux on the PV panel at different inclinations. It can be found that the values fluctuated in the range of 14–17 kW/m$^2$ in Case 1 and 7–9 kW/m$^2$ in Case 5 respectively. The measured incident

**Table 3**
Temperature difference and failure position at photovoltaic panel first failure.

| Experimental conditions | Center point temperature (°C) | | Surface temperature difference (°C) | | | Maximum temperature difference (°C) and failure position |
|---|---|---|---|---|---|---|
| | Fireward surface | Backfire surface | Upper edge | Right edge | Bottom edge | |
| 0°-1 | 111 | 45 | 71 | 66 | 62 | 71 (upper edge) |
| 0°-2 | 117 | 38 | 73 | 71 | 66 | 73 (upper edge) |
| 0°-3 | 104 | 45 | 74 | 69 | 67 | 74 (upper edge) |
| **Average** | **111** | **43** | **73** | **69** | **65** | **73** |
| 15°-1 | 117 | – | 77 | 80 | 72 | 80 (left edge) |
| 15°-2 | 114 | 35 | 69 | 72 | 58 | 72 (left edge) |
| 15°-3 | 106 | 39 | 72 | 72 | 59 | 72 (right edge) |
| **Average** | **112** | **41** | **73** | **75** | **63** | **75** |
| 30°-1 | 107 | 35 | 88 | 95 | 64 | 95 (right edge) |
| 30°-2 | 109 | 50 | 77 | 74 | 82 | 82 (upper edge) |
| 30°-3 | 109 | 57 | 67 | 83 | 82 | 83 (left edge) |
| **Average** | **109** | **46** | **77** | **84** | **76** | **84** |
| 45°-1 | 148 | 77 | 50 | 55 | 76 | 76 (left edge) |
| 45°-2 | 143 | 57 | 56 | 59 | 56 | 59 (upper edge) |
| 45°-3 | 122 | 63 | 56 | 47 | 54 | 56 (upper edge) |
| **Average** | **138** | **66** | **54** | **54** | **62** | **62** |
| 60°-1 | 140 | 81 | 62 | 51 | 51 | 62 (upper edge) |
| 60°-2 | 121 | 61 | 52 | 58 | – | 58 (upper edge) |
| 60°-3 | 121 | 65 | 69 | 42 | 38 | 69 (intersection aera) |
| **Average** | **127** | **67** | **61** | **50** | **44** | **61** |

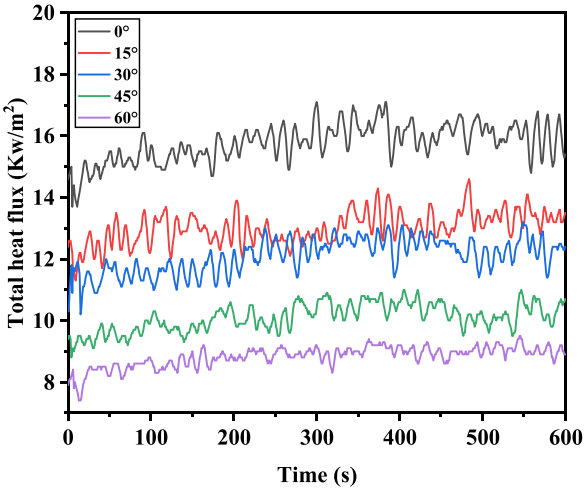


**Fig. 10.** The measured incident heat fluxes at the top of PV panel with different inclinations.

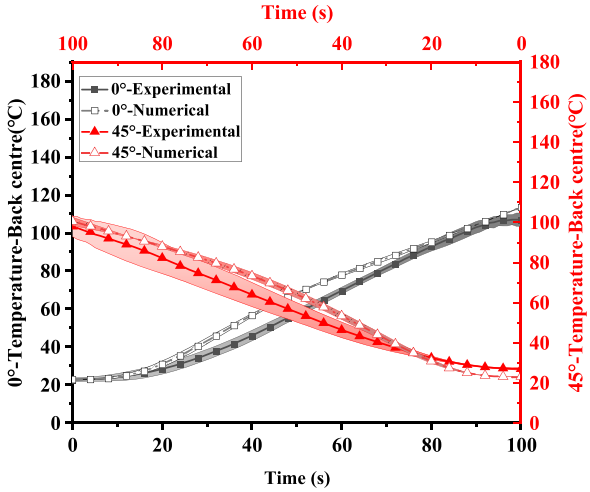


**Fig. 11.** Comparison of the central temperature of TPT between experimental and numerical conditions in Cases 1 and 4.

**Table 4**
The incident heat fluxes at the first failure time.

| Working Conditions | Heat flux (kW/m$^2$) | | | |
|---|---|---|---|---|
| | Test 1 | Test 2 | Test 3 | average |
| Case 1 (0°) | 13.8 | 14.5 | 15.0 | 14.4 |
| Case 2 (15°) | 12.2 | 12.5 | 11.6 | 12.1 |
| Case 3 (30°) | 9.9 | 10.6 | 11.0 | 10.5 |
| Case 4 (45°) | 9.4 | 9.0 | 9.8 | 9.4 |
| Case 5 (60°) | 8.6 | 7.9 | 8.2 | 8.2 |

heat fluxes of PV panels at the moment of fracture are presented in Table 4, and the heat flux varies significantly when the tilt angle changes. As the PV panels were continuously tilted, the heat flux in the upper part of the PV panels decreased, and the minimum heat flux for failure was 7.9 kW/m$^2$, which occurred in Case 5.

### 3.2. Numerical results and discussion

In order to reveal the thermal behavior mechanism, the results of the first 100 s of the experiments were selected for numerical simulation, due to the first breakage of glass in PV panels occurring during this period. The experimental temperatures measured by TC 9 (center of back surface) and the predicted temperatures in Cases 1 and 4 are shown in Fig. 11: the experimental and simulated mean values are represented by solid and dashed lines, respectively, with the corresponding standard errors indicated by shaded areas. Compared with the experimental results, the average error for all the cases was 13.5 % in the thermal model of the PV panels, indicating that the thermal model was capable of predicting the PV panel temperature under fire conditions. However, it should be mentioned that the numerical results are slightly higher than experiments, which may be caused by the gas bubbles of EVA and expansion of the TPT (Fig. 7(b) and (c)), resulting in the temperature of the internal layers not being transferred to the back sheet, which has not been taken into account in the thermal model.

The temperature distributions of the exposed PV panel glass surface at breakage times (29 s and 68 s in Test 2, Case 1 and Test 3, Case 4) are illustrated in Fig. 12. It can be observed that, at the moment of breakage, the temperature fields in numerical model are similar: the temperatures of the exposed areas are much higher than covered areas, and the temperature differences between the exposed and shaded regions,

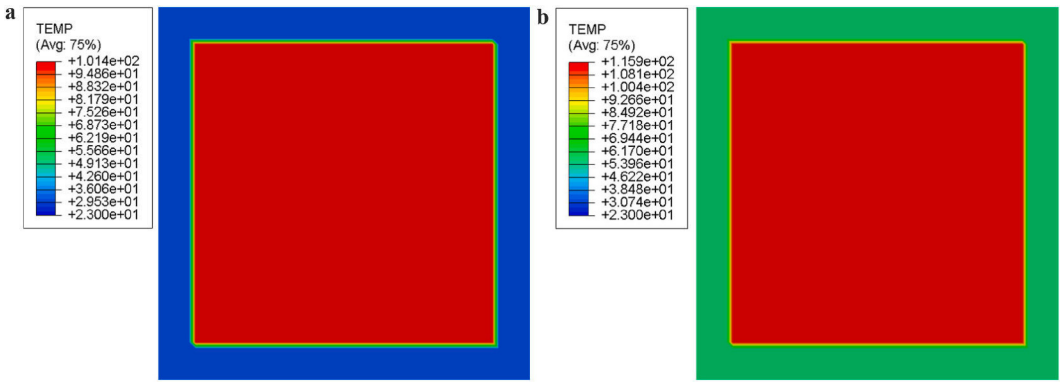


**Fig. 12.** The temperature field (°C) of the exposed PV panel glass surface at the time of breakage: Test 2 (Case 1, left) and Test 3 (Case 4, right).

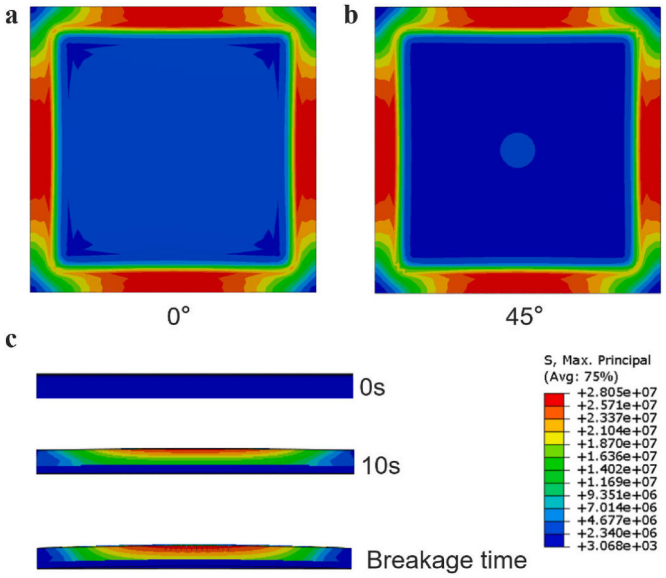


**Fig. 13.** (a)–(b) The planar direction stress fields at the final calculated step just before the crack occurrence in Test 3 of Case 1 and Test 3 of Case 4; (c) Stress variance at different times in Test 2 of Case 2.

**Table 5**
The summary of breakage times.

| Working condition | Cracking Time (s) | Modelling Time (s) |
|---|---|---|
| 0°-1 | 38 s | 33 s |
| 0°-2 | 32 s | 29 s |
| 0°-3 | 37 s | 30 s |
| **Average** | 36 s | 31 s |
| 15°-1 | 34 s | 27 s |
| 15°-2 | 29 s | 29 s |
| 15°-3 | 36 s | 31 s |
| **Average** | 33 s | 29 s |
| 30°-1 | 38 s | 32 s |
| 30°-2 | 46 s | 43 s |
| 30°-3 | 36 s | 26 s |
| **Average** | 40 s | 34 s |
| 45°-1 | 72 s | 54 s |
| 45°-2 | 60 s | 49 s |
| 45°-3 | 54 s | 68 s |
| **Average** | 62 s | 57 s |
| 60°-1 | 77 s | 84s |
| 60°-2 | 68 s | No |
| 60°-3 | 67 s | 95 s |
| **Average** | 71 s | 90 s |

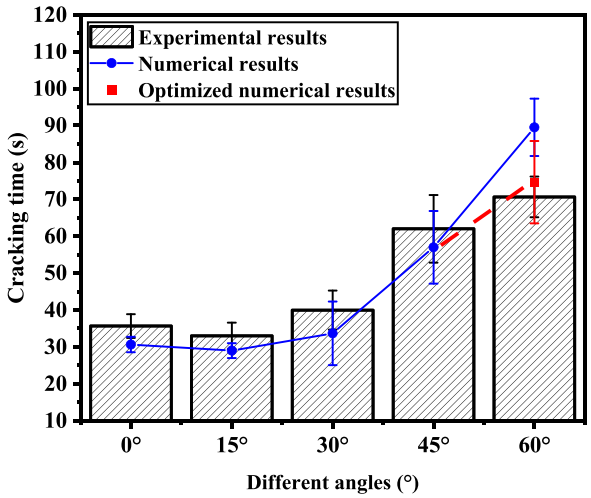


**Fig. 14.** Comparison of the first failure time of PV panels between experimental, numerical and modified numerical results.

defined as follows, were 72 °C and 61 °C in Cases 1 and 4, respectively.

As previously highlighted, the simulation was aimed to investigate the stress distributions for various angles of PV panels and calculate the breakage times. The thermal stresses were calculated by means of sequentially-coupled thermo-mechanical analyses by assuming the mechanical properties shown in Table 1; the element size used for the heat transfer model was retained in the mechanical model. The stress fields were determined by applying the temperature variation at each node in glazing. It is assumed that the initiation of cracks in the glass pane occurs when the maximum principal stress surpasses the strength of glass [47]. The use of material properties as for room conditions was justified by the magnitude of measured temperatures during the experiments.

The stress fields of PV panels in Test 3 of Case 1 and Test 3 of Case 4, as well as the stress variation over time in Test 2 of Case 2, are shown in Fig. 13 at the final calculated step before crack initiation. For PV panels with various inclinations, the maximum principal stresses were observed at the high-temperature gradient edge, which agrees with experimental results. It can be found that in Fig. 13(c) that the tensile stress increased on the exposed side as the heating progressed, particularly at the regions where cracks were most likely to initiate.

As depicted in Table 5 and Fig. 14, the average first failure times of the PV panel models were 31, 29, 34 and 57 s from 0° to 45°, respectively, with an average error less than 15 %. However, the relatively large errors in Case 5, where the calculated time prominently exceeds experimental result should be noted. This was caused by the assumption of uniform thermal loading: at 60° condition, the PV panel was significantly more unevenly heated due to the excessive PV panel inclinations,

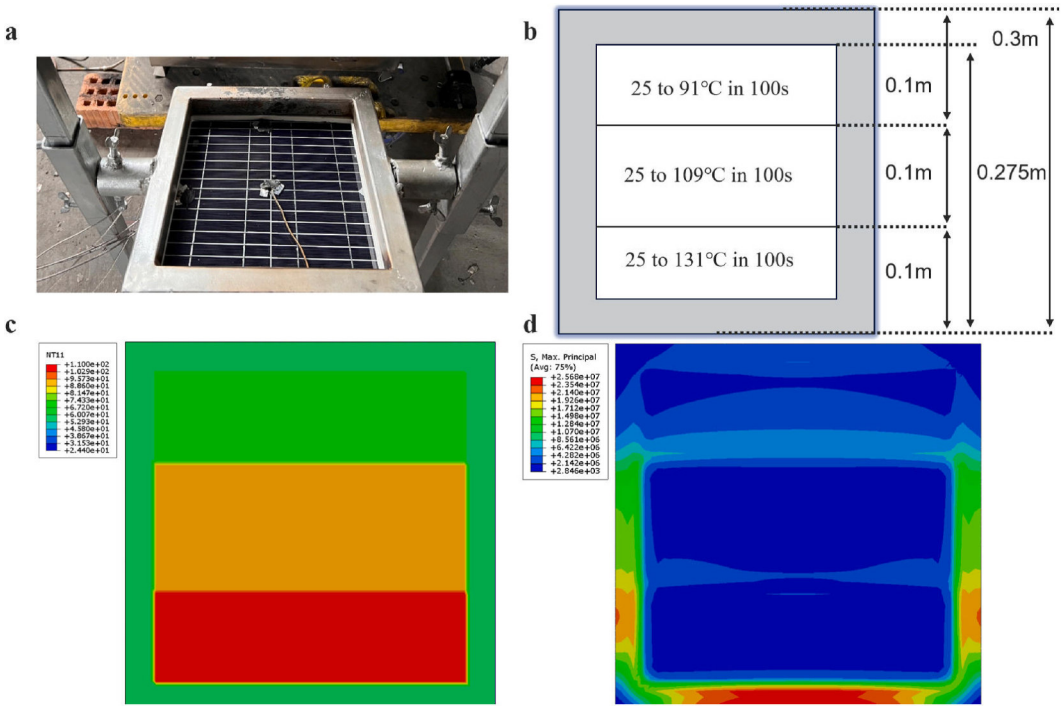


**Fig. 15.** (a) PV panel in Case 5; (b) A simple assumption of a three-layer rising temperature; (c) Temperature distribution and (d) Maximum principal stress distribution in glazing in PV panels before crack initiation.

which suggests the assumption of uniform thermal loading with 60° or more inclination may not work in FEM model.

Moreover, TC 6, obstructed by the frame (Fig. 15(a)), yields temperatures lower than actual values, hence leading to a significant discrepancy in failure time during the simulation. Therefore, in this section, the above temperature errors were corrected using an assumption of a three-layer rising temperature. A square PV pane of 0.0047 × 0.3 × 0.3 $m^3$, the same as the experiments, was used in the optimized simulation. It can be found that in Fig. 15(b), the edge of the pane is covered by a frame with a width of 0.025 m. The central section of the PV panel was further divided into three regions with different heating rates. Taking Test 2 of Case 5 as an example, the panel was heated for 100 s, and the final temperatures in the upper, middle, and lower sections were 91 °C, 109 °C, and 131 °C (assumed temperature by linear calculation), respectively. Fig (c) and (d) show the calculated temperature fields and maximum principal stress, respectively. It can be found that the temperature of the lower part is significantly higher than the other two parts; therefore, the maximum principal stress reaches its maximum value in the center part of the lower edge. Fig. 14 show the optimized numerical results, it can be seen that under this assumption, the simulated failure times are 83 s, 62 s, and 79 s, respectively, with an average error of 5.3 % from the experiment, proving a very good validity of the model.

In addition, as depicted in Fig. 16(a), the PV panel was tilted at an angle of 75° and heated using a radiant panel at the same condition in a pre-test. We found that the failure time was 68 s, and the average failure time of PV panels at 60° was 71s. The difference in failure time between the two was not significant, with the average error smaller than 5 %. Furthermore, based on the simple assumption of a three-layer rising temperature used in the 60° condition, the central portion of the PV panel was divided into three regions in which the heating rates were different. The temperature is assumed to be a linear distribution and the final temperatures in the upper, middle, and lower regions were 81 °C, 119 °C, and 141 °C. As seen in Fig. (b), the result showed that the first failure time of the PV panel at 75° condition was 76 s, which is not significantly different from the average first failure time at 60°. Therefore, we did not select a larger range of angles for this experiment.

In this experiment, the decomposed of backsheet (TPT) was also obsevered. In actual application scenarios, the PV panel is placed under repeated mechanical and environmental stress and so it must perform its role to ensure the overall longevity of the entire panel. Therefore, the backsheet failure of PV panel is another major issue. A backsheet, usually made of a polymer or a combination of polymers, is used to cover the back of solar PV modules. The main function of this layer is to provide electrical isolation of internal circuitry with the external environment. As a result, any defects or failures can have a detrimental impact on PV module performance. The most common result of backsheet failure is ground faults due to reduced insulation resistance. This often leads to the inverter shutting down, causing significant power loss. In addition to performance loss, ground faults can also lead to safety issues and fire hazards for the whole system. Other potential failures include cracking of the inner or outer layer, delamination, and yellowing. A cracked backsheet no longer presents an effective barrier against moisture and air. This can lead to corrosion of ribbon connections and busbars within the internal circuit. Corrosion will cause hotspots, which means that energy is dissipated in the form of heat, causing additional power loss. These potential failure risks should be taken seriously.

As discussed above, high temperatures greatly influence the performance of PV panels, including the thermal decomposition of combustible materials and the rupture of glass in PV panels. Moreover, excessive heat decreases the energy output of the solar cells, which was proved by Fouad's work [62]. They found that the efficiency of crystalline solar cells falls by roughly 0.5 % per 1 °C increment in cell temperature. Therefore, potential thermal management strategies are essential for regulating the temperature of PV panels. The cooling methods could be divided into active (such as enhanced cooling techniques) and passive (such as phase change materials (PCMs)) types.

One of the active cooling techniques is air cooling, which employs the thermal characteristics of air to dissipate heat from the PV panels. The temperature control and system performance of PV panels could be achieved through the heat sink, air collector or ventilator. Passive approaches, such as PCMs, could be inserted at the back of the panels to

(a) PV panel at 75° condition.

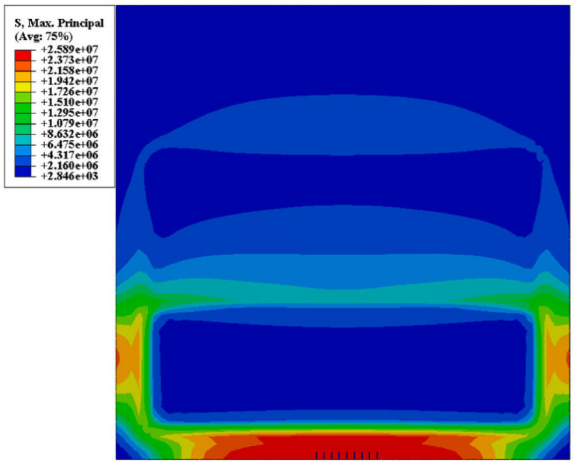


(b) Maximum principal stress distribution in glazing in PV panels at the time of crack initiation.

**Fig. 16.** (a) PV panel at 75° condition. (b) Maximum principal stress distribution in glazing in PV panels at the time of crack initiation.

prevent the temperature increment of PV panels. PCMs absorb the excess thermal energy through reversible phase transition [63], so that preventing efficiency reduction due to temperature increase. Typical PCMs include paraffin, fatty acids and salt hydrates, and new types of PCMs, such as nano-enhanced and composite PCMs are also being utilized in PV panel heat dissipation. These measures could be used in PV panel thermal management, and more research is needed in the field of PV cooling. Moreover, it's valuable to explore the possibility of cooling methods being used in the field of PV fire safety areas.

## 4. Conclusions

In this study, the impact of various inclinations on the thermal behavior of photovoltaic panels was investigated through 15 tests. A well-designed frame made of galvanized steel square tube and the radiant panel were made to model the five different conditions, and the glass breakage within PV panels was studied. Several critical parameters, such as the thermal behavior, surface temperatures, incident heat flux and failure time, were obtained. It was determined that inclinations had a significant impact on both failure time and thermal behaviour. Furthermore, using the measured temperature as thermal loading inputs, a numerical model was implemented to reveal the PV panel failure mechanism. Failure and crack initiation times are in reasonable agreement with the experimental results. The primary conclusions are as follows.

(1) For PV panels under thermal radiation, the glass cracks were normally initiated at the edge of the maximum temperature difference on the fire-exposed surface; while due to the existence of converged ribbons at the bottom of PV panel, cracks were prone to initiating there rather than panel edges when the inclination was larger than 45°. Furthermore, combustible gas bubbles were found between the glass layer and the solar cell layer, as well as between the backplate and the solar cell layer, which could be potentially ignited with a sparker or in a real fire.
(2) The average time for PV panels first failure showed an increasing trend when the panels inclined from 0° to 60°. The time to failure increased significantly when the PV panels were further tilted beyond 30°, which is a critical inclination angle for the thermal failure of the PV panel.
(3) Temperature gradients in glazing are the primary reason for PV panels failure initiation even though the panels are mounted at different angles. Although failure times were different across the cases, the critical temperature differences were close, ranging from 61 to 84 °C, and the majority of cracking occurred within 8–15 kW/m$^2$.
(4) For the FEM heat transfer model, the average error of temperature distributions for all the cases was 13.5 % compared with the experimental results. Considering the difficulties caused by the gas bubbles of EVA and expansion of the TPT, this agreement suggested that the thermal model could predict the PV panel

temperature fields. The breakage times calculated were also in agreement with experimental results, validating the numerical model. The assumption of a three-layer rising temperature is proved suitable for the cases with large inclinations.

## CRediT authorship contribution statement

**Yu Wang:** Writing – review & editing, Supervision, Project administration, Methodology, Investigation, Funding acquisition, Conceptualization. **Chengming Xiao:** Writing – review & editing, Writing – original draft, Validation, Software, Methodology, Investigation, Formal analysis. **Chiara Bedon:** Writing – review & editing, Methodology.

## Declaration of competing interest

None.

## Acknowledgments

The authors would like to acknowledge the National Key R&D Program of China (2023YFE0116700), National Natural Science Foundation of China (Grant No. 52176137), Fundamental Research Funds for the Central Universities (WK2320000051), University of Science and Technology of China Start Research Funding (KY2320000023). The Italian Ministry of Foreign Affairs and International Cooperation (CN24GR03) is also acknowledged. The assistance in the experiments from Mr Liangjie Ma is appreciated.

## Appendix A. Supplementary data

Supplementary data to this article can be found online at https://doi.org/10.1016/j.ijthermalsci.2024.109489.

## Data availability

The authors do not have permission to share data.

## References

[1] The International Energy Agency, Snapshot of global PV markets. https://iea-pvps.org/snapshot-reports/snapshot-2023/, 2023.
[2] M. Victoria, N. Haegel, I.M. Peters, et al., Solar photovoltaics is ready to power a sustainable future, Joule 5 (5) (2021) 1041–1056.
[3] 61730-1: I, Ed 1–Photovoltaic (PV) Module Safety Qualification–Part 1: Requirements for Construction, International Electrotechnical Commission, Geneva, 2016.
[4] E. Standard, 50583-1: Photovoltaics in Buildings—Part 1: BIPV Modules, CENELEC, Bruxelles, 2016.
[5] M. Shipp, C. Holland, D. Crowder, et al., Fire safety and solar electric/photovoltaic systems, International Fire Prof 6 (2013) 12–17.
[6] N. Groom, N. Balu, Walmart Sues Tesla for Negligence after Repeated Solar System Fires, REUTERS, 2019.
[7] S. Blazey, Fire and Solar PV Systems–Investigations and Evidence: Report (2017).
[8] R. Backstrom, D. Dini, Firefighter safety and photovoltaic installations research project, Reliability of photovoltaic cells, modules, components, and systems V 8472 (2012) 84720K.
[9] R. Backstrom, D. Sloan, Effect of Rack Mounted Photovoltaic Modules on the Fire Classification Rating of Roofing Assemblies Phase 2[R], 2009. Illinois, USA.
[10] M. Lamberto, C. Piergiacomo, P. Giuseppe, et al., Fire risk related to the use of PV systems in building facades (2016) 05001, https://doi.org/10.1051/matecconf/20164605001.
[11] N A F Mohd Nizam Ong, M.A. Sadiq, M.S.M. Said, et al., Fault tree analysis of fires on rooftops with photovoltaic systems, J. Build. Eng. 46 (2022) 103752.
[12] S. Lu, B.T. Phung, D. Zhang, A comprehensive review on DC arc faults and their diagnosis methods in photovoltaic systems, Renew. Sustain. Energy Rev. 89 (2018) 88–98.
[13] Y.N. Qiu, T.R. Betts, R. Gottschalg, Electrical mismatch within single junction amorphous silicon and micromorph tandem thin film PV modules[C], in: 2009 34th IEEE Photovoltaic Specialists Conference (PVSC), IEEE, 2009, pp. 911–916.
[14] F. Spertino, J.S. Akilimali, Are manufacturing $ I $–$ V $ mismatch and reverse currents key factors in large photovoltaic arrays? IEEE Trans. Ind. Electron. 56 (11) (2009) 4520–4531.
[15] A. Wang, Y. Xuan, Close examination of localized hot spots within photovoltaic modules, Energy Convers. Manag. 234 (2021) 113959.
[16] P. Cancelliere, V. Puccia, G. Longobardo, et al., Behavior of the electrical parameters of PV modules subject to a flame ignition[C], in: 28th European Photovoltaic Solar Energy Conference and Exhibition, 2013.
[17] T.R. Hull, R.E. Quinn, I.G. Areri, et al., Combustion toxicity of fire retarded EVA, Polym. Degrad. Stabil. 77 (2) (2002) 235–242.
[18] S.S. Nair, A.M. Kulkarni, Experimental study on the flammability of photovoltaic module backsheets, Int. J. Sci. Eng. Res. 9 (5) (2018).
[19] C.L. Chow, S.S. Han, X.M. Ni, A study on fire behaviour of combustible components of two commonly used photovoltaic panels, Fire Mater. 41 (1) (2017) 65–83.
[20] H.-Y. Yang, X.-D. Zhou, L.-Z. Yang, et al., Experimental studies on the flammability and fire hazards of photovoltaic modules, Materials 8 (7) (2015) 4210–4225.
[21] L. Kolodny. Tesla solar panels caught fire at Amazon warehouse in 2018 https://www.cnbc.com/2019/08/23/tesla-solar-panels-caught-fire-at-amazon-warehouse-in-2018-report.html..
[22] Galaviz A. Amazon Fresno warehouse three-alarm fire burns solar panels , stops work https://www.fresnobee.com/news/local/article242015301.html..
[23] Sylvia T. Amazon warehouse fire linked to solar installation https://www.pv-magazine.com/2021/06/11/amazon-warehouse-fire-linked-to-solar-installation/..
[24] Press C S F-A. Fire Causes Partial Roof Collapse At Apple's Giant Data Center In Arizona https://www.cbsnews.com/sanfrancisco/news/fire-causes-partial-roof-collapse-at-apples-giant-data-center-in-arizona/..
[25] J.S. Kristensen, F.B.M. Faudzi, G. Jomaas, Experimental study of flame spread underneath photovoltaic (PV) modules, Fire Saf. J. 120 (2021) 103027.
[26] J.S. Kristensen, B. Jacobs, G. Jomaas, Experimental study of the fire dynamics in a semi-enclosure formed by photovoltaic (PV) installations on flat roof constructions, Fire Technol. 58 (4) (2022) 2017–2054.
[27] J.S. Kristensen, G. Jomaas, Experimental study of the fire behaviour on flat roof constructions with multiple photovoltaic (PV) panels, Fire Technol. 54 (2018) 1807–1828.
[28] J.S. Kristensen, B. Merci, G. Jomaas, Fire-induced reradiation underneath photovoltaic arrays on flat roofs, Fire Mater. 42 (3) (2018) 316–323.
[29] L. Miao, C.-L. Chow, Investigation of burning photovoltaic panels on a double-skin facade with ejecting flame from an adjacent room fire, Indoor Built Environ. 28 (7) (2019) 938–949.
[30] K. Almand, Request for proposals–PV installation best practices review and all hazard assessment, in: Fire Protection Research Foundation, vol. 1, National Fire Protection Association, 2012.
[31] 61730–2 I, Photovoltaic (PV) module safety qualification–Part 2: requirements for testing, Int. Electrotech. Comm. (2016).
[32] Ul, Standard for Flat-Plate Photovoltaic Modules and Panels[M], 2002.
[33] C. Erban, BIPV Standard EN 50583 Photovoltaics In Buildings Released, Energy Build. (2016).
[34] J.S. Kristensen, Fire risk associated with photovoltaic installations on flat roof constructions: experimental analysis of fire spread in semi-enclosures, Fire Techol. (2023).
[35] JGJ 102-2003.Technical specifications for glass curtain wall engineering [s]..
[36] A. Hafez, A. Soliman, K. El-Metwally, et al., Tilt and azimuth angles in solar energy applications–A review, Renew. Sustain. Energy Rev. 77 (2017) 147–168.
[37] A.K. Yadav, S. Chandel, Tilt angle optimization to maximize incident solar radiation: a review, Renew. Sustain. Energy Rev. 23 (2013) 503–513.
[38] A Photovoltaic curtain wall and roof in Zhejiang https://www.vrqjcs.com/p/9a0a86bc240d25ff..
[39] How to protect rooftop solar systems from fire risk https://www.pv-magazine-india.com/2021/03/25/how-to-protect-rooftop-pv-systems-from-fire-risk/..
[40] M.-C. Despinasse, S. Krueger, First developments of a new test to evaluate the fire behavior of photovoltaic modules on roofs, Fire Saf. J. 71 (2015) 49–57.
[41] A.C.Y. Yuen, T.B.Y. Chen, A. Li, et al., Evaluating the fire risk associated with cladding panels: an overview of fire incidents, policies, and future perspective in fire standards, Fire and materials 45 (5) (2021) 663–689.
[42] M. Bonner, G. Rein, Flammability and multi-objective performance of building faades: towards optimum design, International Journal of High-Rise Buildings. (4) (2018).
[43] R. Stølen, T. Li, T. Wingdahl, et al., Large-and small-scale fire test of a building integrated photovoltaic (BIPV) façade system, Fire Saf. J. 144 (2024) 104083.
[44] H. Chen, Y. Wang, Y. Zhang, et al., Crack evolution process of window glass under radiant heating, Fire Mater. 41 (8) (2017) 1016–1026.
[45] L. Li, Q. Xie, X. Cheng, et al., Cracking behavior of glazings with different thicknesses by radiant exposure, Fire and materials 36 (4) (2012) 264–276.
[46] Q. Wang, Y. Wang, Y. Zhang, et al., A stochastic analysis of glass crack initiation under thermal loading, Appl. Therm. Eng. 67 (1–2) (2014) 447–457.
[47] Y. Wang, Q. Wang, Y. Su, et al., Fracture behavior of framing coated glass curtain walls under fire conditions, Fire Saf. J. 75 (2015) 45–58.
[48] D.L.W. Wong, The Fallout of Single Glazing under Radiant Heat Exposure (2011).
[49] C. Bedon, M. Kozlowski, D. Honfi, Thermal assessment of glass facade panels under radiant heating-Experimental and preliminary numerical studies, J. Facade Des. Eng. 6 (3) (2018) 49–64.
[50] Z. Yi, W. Qing-Song, Z. Xiao-Bin, et al., Experimental study on crack of float glass with different thicknesses exposed to radiant heating, Procedia Eng. 11 (2011) 710–718.
[51] Y. Wang, Q. Wang, G. Shao, et al., Fracture behavior of a four-point fixed glass curtain wall under fire conditions, Fire Saf. J. 67 (2014) 24–34.
[52] A. A, Joshi, et al., Fire-induced thermal fields in window glass. II—experiments, Fire Saf. J. (1994).
[53] A. Vedrtnam, C. Bedon, M.A. Youssef, et al., Effect of non-uniform temperature exposure on the out-of-plane bending performance of ordinary laminated glass panels, Compos. Struct. 275 (2021) 114517.

[54] M. Smith, ABAQUS/Standard User's Manual (2009). Version 6.9[J].
[55] Y. Wang, J. Hu, Performance of laminated glazing under fire conditions, Compos. Struct. 223 (2019) 110903.
[56] A method for calculating the hot spot temperature of photovoltaic modules, CN106066916B (2019-04-05).
[57] A PV panel company in Shenzhen https://shop358925ez8n797.1688.com/..
[58] Committee N S. Ethylene-vinyl acetate copolymer (EVA) film for PV module https://openstd.samr.gov.cn/bzgk/gb/newGbInfo?hcno=1D0A4045B78B4A8C1012951719D3DF3E..
[59] Ministry of Industry and Information Technology. Glass for solar cell module https://hbba.sacinfo.org.cn/stdDetail/c150691d9f862dd7740d246fd3722774..
[60] J. Lai, T. Perazzo, Z. Shi, et al., Optimization and performance of high-resolution micro-optomechanical thermal sensors, Sensor Actuator Phys. 58 (2) (1997) 113–119.
[61] G. Osayemwenre, E. Meyer, Thermal decomposition of EVA composite encapsulant of single junction amorphous silicon photovoltaic (PV) module, J Ovonic Res 10 (6) (2014) 221–229.
[62] M.M. Fouad, L.A. Shihata, E.S.I. Morgan, An integrated review of factors influencing the perfomance of photovoltaic panels, Renew. Sustain. Energy Rev. 80 (2017) 1499–1511.
[63] T. Ma, Z. Li, J. Zhao, Photovoltaic panel integrated with phase change materials (PV-PCM): technology overview and materials selection, Renew. Sustain. Energy Rev. 116 (2019) 109406.